Crystal and Crystallites Structure of Natural Rubber and Synthetic cis- 1,4-Polyisoprene by a New Two Dimensional Wide Angle X-ray Diffraction Simulation Method. I. Strain-Induced...

ARTICLE *in* MACROMOLECULES · MAY 2013

Impact Factor: 5.8 · DOI: 10.1021/ma400420k

Macromolecules

Article

pubs.acs.org/Macromolecules

Crystal and Crystallites Structure of Natural Rubber and Synthetic *cis*-1,4-Polyisoprene by a New Two Dimensional Wide Angle X-ray Diffraction Simulation Method. I. Strain-Induced Crystallization

Justin Che,* Christian Burger,* Shigeyuki Toki,* Lixia Rong, and Benjamin S. Hsiao

Department of Chemistry, Stony Brook University, Stony Brook, New York 11794-3400, United States

Sureerut Amnuaypornsri and Jitladda Sakdapipanich

Department of Chemistry and Center of Excellence for Innovation in Chemistry, Faculty of Science, Mahidol University, Bangkok 10400, Thailand

ABSTRACT: A novel two-dimensional simulation method to analyze a wide-angle X-ray diffraction (WAXD) pattern is applied to crystal and crystallites of strain-induced crystallization (SIC) of unvulcanized natural rubber (NR) and synthetic polyisoprene rubber (IR) at −50 °C. The unit cell dimensions of SIC were determined by calculation of scattering factors based on atomic coordinates and symmetry, and were compared with the observed data. The unit cell dimensions are the same in NR and IR, and do not change during extension. The crystallites' dimensions in NR and IR are almost the same at −50 C. The orientation of crystallites in NR is lower than in IR. The order of crystals in NR is lower than in IR. The crystalline fraction increases with strain because of the increase in the number of crystallites. The onset strain of SIC in NR is smaller than the one in IR. The different behaviors of SIC in NR and IR seem to be caused by the pseudonetwork of NR.

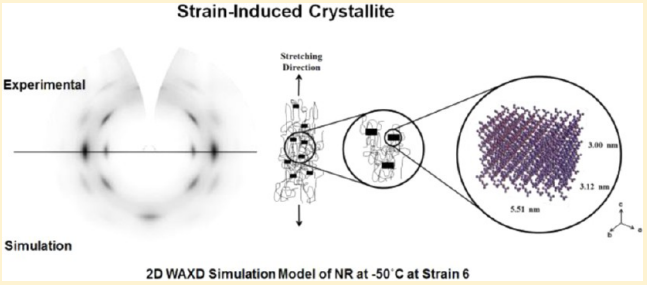

INTRODUCTION

The significant superiority in mechanical properties of natural rubber (NR) as compared to synthetic rubbers has been considered to originate from strain-induced crystallization (SIC) in NR. In 1925, Katz[1,2] discovered crystals in stretched NR (both unvulcanized and vulcanized) by wide-angle X-ray diffraction (WAXD). In the early to mid decades between 1930s to 1950s, the crystal structure of stretched and frozen NR was studied intensively and different models of the unit cell were proposed. Mark and von Susich[3] reported an orthorhombic unit cell composed of four molecular chains, with each chain having two isoprene units. Morss[4] and Bunn[5] proposed a monoclinic unit cell (β = 92°) with an internal screw axis symmetry. Nyburg[6] reported an orthorhombic unit cell and internal glide plane symmetry. Natta and Corradini[7] reported a structure similar to Nyburg's model, but with an orthorhombic unit cell of P_{bac} space group with glide plane symmetry. In 2004, Takahashi and Kumano[8] modified Bunn's model slightly and reported a monoclinic unit cell (β = 93.1°) with space group $P2_1/a$. Immirzi et al.[9] modified Takahashi's model with a pseudo-orthorhombic structure. Rajkumar et al.[10] proposed an orthorhombic unit cell with a space group $P2_12_12_1$ and a glide plane symmetry. These researchers measured unvulcanized NR and unvulcanized deproteinized NR (DPNR) at low temperature such as −25 or −50 °C. The samples were stretched 5−8 times its original length and then set to a sample fixture. This sample with the fixture was frozen and exposed to X-rays for several hours in order to acquire strong X-ray diffraction intensities measured by conventional X-ray instruments. These researchers assumed that SIC can be treated as a fiber symmetry system.

On the other hand, the mechanical properties and strain dependency of SIC has been studied extensively since the 1940s. Gent[11] reported that the stress of peroxide vulcanized NR, after stretching to a certain strain, relaxes to zero in a short period of time at −26 °C. During the stress relaxation, the volume of the sample decreases significantly. This suggests that SIC is accompanied with stress relaxation. SIC of NR starts at strain around 2.0 and its crystalline fraction reaches around 30% of all the molecular chains at room temperature. Around 70% of the molecules still remain amorphous even at the highest strain.[12−15] Synchrotron X-ray makes it possible to measure stress−strain relation and WAXD pictures simultaneously. SIC increases with strain during extension and delays to diminish with decreasing strain during retraction. The fiber axis of crystals (*c*-axis) is parallel to the extension direction.[13,14] The dimensions of SIC crystals increase slightly along the *c*-axis and decreases along the a- and *b*- axis during extension.[15,16]

Received: February 26, 2013
Revised: May 2, 2013
Published: May 23, 2013

The dimensions of crystallites are also changed with extension with the same trends,[14−16] however, the volume of crystallites remains constant[14] or slightly decrease with strain.[15] Therefore, the increase of crystalline fraction is caused by the increase of the number of the crystallites.[14,15]

Flory[17] elucidated the mechanism of the occurrence of SIC from thermo-mechanics, that is, SIC is caused by the rise of the melting temperature (T_m) due to a decrease in entropy by forced deformation. Therefore, SIC is accelerated at lower temperature because of super cooling conditions. On the other hand, it is known that unvulcanized NR preserved in a refrigerator shows whitening due to crystallization. Since the T_m is around room temperature, and the crystallization temperature (T_c) is around −10 °C, the preserved unvulcanized rubber shows crystallization that can be called as temperature-induced crystallization (TIC). Previous researcher's samples may be affected by TIC, since TIC could be occurred in the sample after the stress relaxes to zero. The initiation of SIC at a certain strain is very fast, such as 60 ms[18] and around 100 ms.[16,19] Therefore, SIC might be completed at a certain strain during extension.

NR is a compound of *cis*-1,4-polyisoprene with functional groups at both chain ends and nonrubber components (6 wt.% in fresh latex and 2 wt.% in solid rubber) including proteins, phospholipids, quebrachitol, stearic acid, metal ions, etc. With these functional groups and nonrubber components, NR forms a pseudonetwork that shows high tensile strength and elasticity.[20−22] On the other hand, synthetic polyisoprene is a polymer melt that shows only a viscous response. Some of the nonrubber components in NR, such as quebrachitol and stearic acid, make crystals and some, such as phospholipids and proteins, make agglomerates or aggregates.[20,21,23] These components and pseudonetworks may become constraints for movement of polymer chains in NR.

Two dimensional WAXD images include information of not only unit cell dimension, atomic coordinates, space group and symmetry, but also crystallite size, crystallite orientation, crystalline fraction and disorder in crystal. Our group has developed a method to analyze whole information in two-dimensional images rather than the integrated one-dimensional data.[24] Burger[24,25] and Mao[26] have applied their two-dimensional WAXD pattern simulation method on collagen, cellulose fibers and propylene-1-butylene random copolymer. The scattering X-ray intensity of an individual (hkl) plane in reciprocal space is directly proportional to the square of the structure factors $F_{hkl}(s)$:

$$I_{hkl}(s) \sim [F_{hkl}(s)]^2 \tag{1}$$

where s is the absolute value of the scattering vector **s**.

We assume simple fiber symmetry in SIC. An orientation distribution function $F(\varphi,\varphi_{hkl})$ can be introduced to calculate the scattering intensity distribution of the entire fiber system $J(s, \varphi)$:

$$J(s, \varphi) = \int_0^{\pi/2} I(s, \varphi_{hkl})F(\varphi, \varphi_{hkl}) \sin \varphi_{hkl}\, d\varphi_{hkl} \tag{2}$$

Here φ and φ_{hkl} denote the polar angle of the fiber and the individual structural unit, respectively. Figure 1 shows the geometric relationships between s and the primary axes of the fiber $J(s, \varphi)$ and individual structural unit $I(s,\varphi_{hkl})$, which is adopted from Ruland.[27]

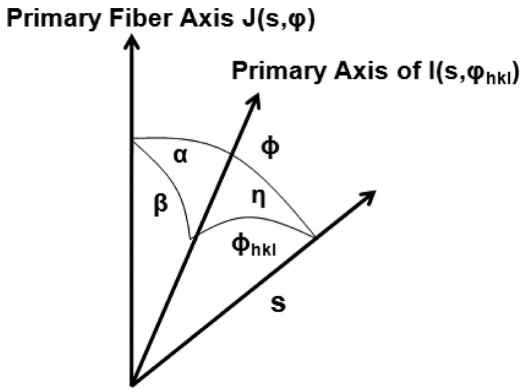

Figure 1. Geometric relationship between the scattering vector s and the primary axes of the fiber $J(s, \varphi)$ and individual structural unit $I(s,\varphi_{hkl})$.

In order to calculate the size of crystallites, we introduce a term w which is the width in the radial direction and its reciprocal value gives an estimate for the average crystallite size. The scattering intensity distribution $I(s,\varphi_{hkl})$ of an (hkl) plane with radius s_{hkl} and polar angle φ_{hkl} can be given as

$$I(s, \varphi_{hkl}) = (4\pi w s_{hkl}^2)^{-1} I_{hkl}(s) \mathrm{Ho}[(s - s_{hkl})/w] \tag{3}$$

where Ho is a one-dimensional normalized peak distribution function. In this simulation work, we used a Lorentzian distribution function that takes the form $\mathrm{Ho}(t) = (1 + \pi^2 t^2)^{-1}$.

In order to estimate the orientation of crystallites, we introduced a term $g(\beta)$ which is the orientation distribution function, where β is the angle between the primary fiber axis and the primary axis of the structural unit. In this simulation, we used a modified Onsager distribution function for $g(\beta)$ that was proposed by Burger:[25]

$$g(\beta) = p_0 + (1 - p_0)p \cosh(p \cos \beta)/\sinh(p) \tag{4}$$

where p_0 is the isotropic unoriented fraction, and p is the width of the distribution of the oriented fraction. The function $F(\varphi,\varphi_{hkl})$ can now be written as

$$F(\varphi, \varphi_{hkl}) = p_0 + (1 - p_0)(p \cosh(p \cos \varphi \cos \varphi_{hkl}) / \sinh(p))I_0(p \sin \varphi \sin \varphi_{hkl}) \tag{5}$$

where I_0 is the modified Bessel function of the first kind of order 0. In this case, the Hermans' orientation factor P_2 is given by:[25]

$$P_2 = (1 - p_0)\{1 - 3p^{-1}[\coth(p) - p^{-1}]\} \tag{6}$$

P_2 is equal to 1 for a perfectly oriented system parallel to the stretching direction, 0 for random orientation, and −0.5 for a perfected oriented system perpendicular to stretching direction. The shape of the crystal can be obtained from the combination of the size and orientation of the crystal.

In order to estimate the crystal lattice disorder, we introduce the Debye−Waller factor (DWF), which corrects for lattice disorder and displacement due to thermal motion The DWF describes the lattice vibrations on Bragg peak intensities and can be given by[28,29]

$$\mathrm{DWF} = \exp(-Bs^2) \tag{7}$$

where B is proportional to the mean square displacement of the atoms, and s is the scattering vector. A highly ordered crystal

dx.doi.org/10.1021/ma400420k | Macromolecules 2013, 46, 4520−4528

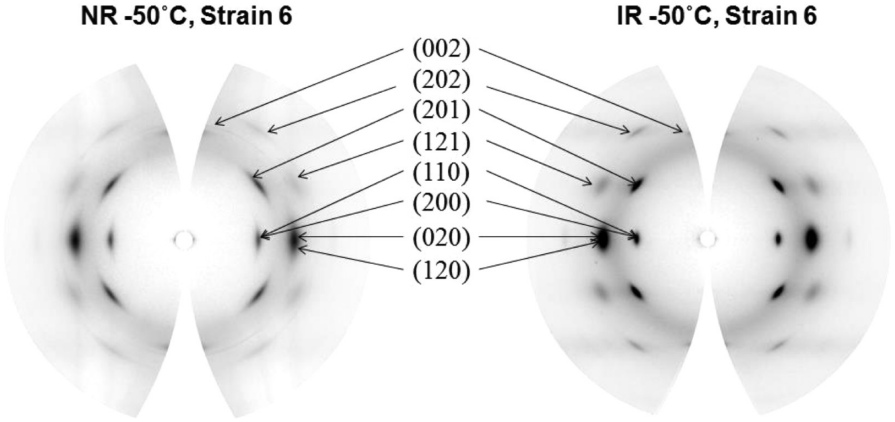

Figure 2. Observed WAXD images, with Fraser correction, at strain 6.0 for unvulcanized NR and IR at −50 °C.

lattice leads to low values for B that does not suppress the scattering intensity.

Finally, the overall fiber averaged intensity distribution can now be written as a combination of eqs 3, 5, and 7:

$$J(s, \varphi) = (4\pi \mathbf{w} s^2_{hkl})^{-1} I_{hkl}(s) H_0[(s - s_{hkl})/w] \times (p_0 + (1 - p_0)(p \cosh(p \cos \varphi \cos \varphi_{hkl})/\sinh(p)) I_0 (p \sin \varphi \sin \varphi_{hkl})) \times \exp(-\mathbf{B} s^2) \quad (8)$$

In order to estimate the crystalline fraction, the amorphous halo could be described by three separate Gaussian intensity distribution functions. The crystalline fraction is determined by taking the ratio of the integrated crystal areas with the total integrated area in the simulated intensity distribution.

This paper aims to apply the two-dimensional WAXD simulation methods to SIC in unvulcanized NR and synthetic *cis*-1,4-polyisoprene (IR) at −50 °C in order to determine the most plausible crystal structure, crystallite size, crystalline fraction, crystallite orientation and crystal disorder.

EXPERIMENTAL SECTION

Materials and Sample Preparation. Two samples were used in this study: unvulcanized natural rubber (NR) and synthetic *cis*-1,4-polyisoprene (IR). Raw NR latex sample was provided by the Thai Rubber Latex Company, Thailand. The fresh NR latex was preserved in ammonia for 3 months at room temperature. The preserved NR was then casted on glass dishes and dried in an oven at 60 °C for 48 h. The synthetic IR used in this study was IR2200 manufactured by JSR. Both of these samples were dissolved in toluene and then casted onto glass dishes. After the evaporation of the solvent, the films created were 1 mm in thickness.

Prior to stretching, the samples were precut into dumbbell-like shapes prior to deformation. The total lengths of the samples were 50 mm. The narrow section of the dumbbell shaped samples were 30 mm in length and 4 mm in width.

Time-Resolved WAXD Measurements and Tensile Deformation. Stress−strain measurements were recorded simultaneously with the time-resolved WAXD measurements during tensile deformation. The strain is defined as the difference of the deformed length and the original length divided by the original length $((l - l_o)/l_o)$. A modified Instron 4442 tensile stretching instrument was used that allowed the uniaxial and symmetric deformation of the sample, while monitoring the structural changes of the sample by illuminating the same sample position during deformation. The samples were deformed up to strains of 6.0 at a stretching rate of 10 mm/min. Tensile deformation was carried out at −50 °C. The samples were set in a heat chamber at −50 °C for 3 min before stretching. The time for stretching is about 20 min. This condition does not allow for the additional effect of temperature and time.

Synchrotron X-ray measurements were carried out at the X27C beamline in the National Synchrotron Light Source (NSLS), Brookhaven National Laboratory (BNL). The X-ray wavelength was set at 1.371 Å. Two-dimensional (2D) wide-angle X-ray diffraction (WAXD) patterns were acquired using a MAR-CCD detector. The acquisition time for each frame was 30 s. Al_2O_3 standard was used to calibrate the scattering angle. The sample-to-detector distances for WAXD was 114 mm. X-ray data analysis was performed using the software Polar (Stony Brook Technology and Applied Research, Stony Brook, New York). All diffraction signals were corrected for beam fluctuations and background scattering. It is to be noted that the observed WAXD patterns were also corrected for the distortion due to the curvature of the Ewald sphere (Fraser correction[30]).

RESULTS AND DISCUSSION

The experimentally obtained, with Fraser corrected, WAXD images at strain 6.0 for unvulcanized NR and IR at −50 °C are shown in Figure 2. The images were obtained for 30 s exposing time. The sample may not have the influence of TIC and stress relaxation. Since the T_g of NR and IR (−70 and −65 °C, respectively) are close to the measuring temperature, the stresses at the strain 6.0 are more than 10 MPa. The detail of stress−strain relation and mechanism of SIC at low temperature will be discussed elsewhere. The peaks are named by the index of the diffraction planes of crystal according to previous researcher's data.[9] With the Fraser correction, the patterns show an empty area along the meridian where the intensity distribution will not intersect with the Ewald sphere. In this case, information regarding the (001), (002) crystal plane peaks, and partial information about the crystal size along the *c*-axis may be lost. Trabelsi et al.[14] and Tosaka et al.[16,19] built a stretching machine that can be tilted to the X-ray in order to obtain information along the meridian. They confirmed that the presence of the (002) plane peak in the crystal, along with the absence of the (001) peak. The peak positions between the NR and IR samples look similar, even though NR and IR are of different origin and stereoregularity. The WAXD pattern shown for this IR sample only contains the SIC of pure *cis*-1,4-polyisoprene, since no impurity is included in IR. On the other hand, it is clear that the shapes of the crystal peaks are different (round and crescent) between the two samples. These differences are attributed to the size, orientation, and disorder of the crystal and crystallites, which affects the shapes along the lateral and phi direction. The peak positions of (110) and (200) are close to each other. It is impossible to separate the

dx.doi.org/10.1021/ma400420k | *Macromolecules* 2013, 46, 4520−4528

intensity of these unit cell planes from the 2D images. The peaks (020) and (120) are of the same situation. Immirzi[9] showed the close relations of these two peaks in their table of structure factors.

In order to determine the unit cell dimensions, space group and space symmetry, we integrated the 2D images into the one-dimensional profile in Figure 3. A general software for

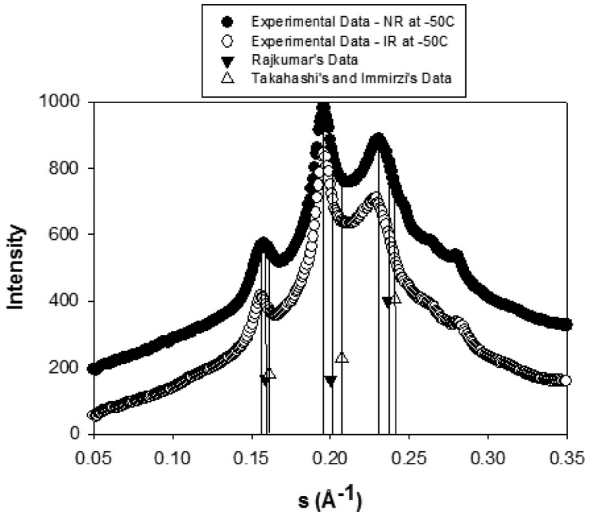

Figure 3. Scattering peak positions and relative intensities in one-dimensional profile of Takahashi–Immirzi's data (△), Rajkumar's data (▼), and our observed profile of NR and IR.

crystallography, Bruker TOPAS, was applied to analyze the one-dimensional profile and concluded that the strain-induced crystallite is an orthorhombic unit cell with space group $P2_12_12_1$. This conclusion is consistent with Rajkumar et al.[10]

The reported crystal peak positions and relative intensities of (200), (201), and (120) by Takahashi,[8] Immirzi,[9] and Rajkumar[10] are presented as points and bars in Figure 3. Figure 3 also shows our observed data on the NR and IR diffraction profiles, including the amorphous diffraction (called as amorphous halo). Takahashi did not show the peak positions in his table of observed and calculated structure factors, but Immirzi analyzed Takahashi's data and determined the Bragg *d*-spacings. Therefore, they both started from the same observed data, but their conclusions were different, i. e., Takahashi chose a monoclinic unit cell and Immirzi selected a pseudo-orthorhombic unit cell. On the other hand, the peak positions and measured structure amplitudes for Rajkumar's observed data is shown in their table 1. The peak positions of Takahashi–Immirzi, Rajkumar, and our observed data are slightly different from each other. The difference in peak positions lead to different atomic coordinates and unit cell dimensions.

Our observed NR and IR profiles showed the same peak positions as shown in Figure 3. The crystal unit cell of *cis*-1,4-polyisoprene seems to be not affected by the stereoregularity and impurity differences. The observed WAXD intensities of NR at different strains are shown in Figure 4. The WAXD intensities are composed of amorphous halo and crystalline peaks. At strain 0, all molecules are in the amorphous state. SIC is observed at higher strains, and the peak positions do not change during extension.

Previous researchers picked up more than 40 peak positions in order to determine the unit cell dimensions and atom coordinates. On the other hand, we focused only on the three strong peak positions (200), (201), and (120), since the intensities at other positions are significantly weaker. In the case of an orthorhombic unit cell, these three positions are enough to determine the unit cell dimensions. Takahashi and Kumano measured unvulcanized DPNR (3 mm thick and 3 mm wide) with 7 times the extension at −50 °C using a conventional X-ray instrument. Rajkumar et al. measured unvulcanized NR at room temperature by a conventional X-ray instrument, but there was no mention on the extension ratio and the exposing time. In the case of unvulcanized NR at room temperature, it may take several hours in order to acquire enough intensity to analyze the data of more than 6 times the extension, and the stress may decrease quickly.

We adopted the carbon atom coordinates from Rajkumar et al. From the peak positions of (200), (201), (120), we determined our unit cell dimension as a = 13.048 Å, b = 9.391 Å, and c = 8.551 Å. The dimensions of our unit cell are slightly larger than the dimensions of Rajkumar, which are a = 12.586 Å, b = 8.985 Å, and c = 8.205 Å. As a consequence, a linear expansion of unit cell and affine displacements of carbon atoms of Rajkumar's unit cell structure is assumed. Our unit cell model is shown in Figure 5.

Based on our atomic coordinates and unit cell dimensions, the scattering X-ray intensity of an individual (*hkl*) plane in reciprocal space were calculated using eq 1. Table 1 shows the scattering positions s, Bragg spacing d, the total observed and calculated WAXD intensities for each specific (*hkl*) plane of NR at strain 6.0. It is to note that the scattering intensities shown in Table 1 also includes the intensities of the amorphous halo, although previous researchers did not concern the amorphous molecules' contribution.

By comparing the observed and calculated WAXD intensities, these values are in close correspondence with each other, which is an indication that our modified Rajkumar's unit cell structure is a suitable model for SIC of *cis*-1,4-polyisoprene at −50 °C. We have also compared Takahashi's and Immirzi's model, but we have found that the correspondence is not as closely as our modified Rajkumar's model. We also confirmed that calculated and observed of NR at strain 3.0 and 4.0 with our modified Rajkumar's model are very close.

In order to determine crystallites size, crystallites orientation and crystal disorder, we simulate the calculated values with w, p, and B in eq 8 to match the experimentally observed peaks in the 2D WAXD images and its corresponding one-dimensional integration. During the simulation process, w, p, and B were varied to improve the fitting. Each parameter varies the fiber patterns differently, and each individual parameter tells a specific aspect of the crystallite. Varying w will change the width of the peaks along the radial direction, which can tell us information about the sizes of the crystallite. A larger w used in the diffraction pattern indicates a smaller size crystallite in real space. Varying p will change the width of the peaks along phi. A p value close to zero will produce a powder diffraction pattern with rings that have no orientation, whereas a large p value will produce sharp diffraction reflections that have high orientation. Varying B will change the intensity of certain Bragg peaks, where the relative ratios of the diffraction peak intensities can be adjusted. The best combinations of w, p, and B were obtained for each sample at specific strains after matching the simulated pattern to the observed pattern with the highest R^2 value and with R^2 values greater than 0.98.

dx.doi.org/10.1021/ma400420k | *Macromolecules* 2013, 46, 4520–4528

Table 1. Observed and Calculated WAXD Intensities for Each Specific (*hkl*) planes

s (Å^{-1})	d (Å)	I_{obs}	I_{sim}	h	k	l
0.1312	7.622	237.7	237.1	-1	-1	0
				-1	1	0
				1	-1	0
				1	1	0
0.1533	6.524	571	563.2	-2	0	0
				2	0	0
0.1582	6.323	470	469.2	0	-1	1
				0	1	1
0.1758	5.690	476.4	478.6	-1	-1	1
				-1	1	1
				1	-1	1
				1	1	1
				-1	-1	-1
				-1	1	-1
				1	-1	-1
				1	1	-1
0.1866	5.358	640.1	679.6	-2	-1	0
				-2	1	0
				2	-1	0
				2	1	0
0.1928	5.187	918.2	878.2	-2	0	1
				2	0	-1
				-2	0	1
				2	0	-1
0.2130	4.695	750.9	768.7	0	-2	0
				0	2	0
0.2203	4.540	878.3	886.6	-2	-1	1
				-2	1	1
				2	-1	1
				2	1	1
				-2	-1	-1
				-2	1	-1
				2	-1	-1
				2	1	-1
0.2263	4.418	983.4	989.7	-1	-2	0
				-1	2	0
				1	-2	0
				1	2	0
0.2339	4.276	832.4	806.0	0	0	2
				0	0	-2
0.2534	3.947	463.3	476.4	-3	-1	0
				-3	1	0
				3	-1	0
				3	1	0
0.2548	3.925	461.7	469.4	-1	-2	1
				-1	2	1
				1	-2	1
				1	2	1
0.2624	3.811	432.0	408.4	-2	-2	0
				-2	2	0
				2	-2	0
				2	2	0
0.2682	3.729	383.7	352.9	-1	-1	2
				-1	1	2
				1	-1	2
				1	1	2
				-1	-1	-2
				-1	1	-2
				1	-1	-2
				1	1	-2
0.2791	3.583	368.4	303.4	-3	-1	1
				-3	1	1
				3	-1	1
				3	1	1
				-3	-1	-1
				-3	1	-1
				3	-1	-1
				3	1	-1
0.2796	3.576	367.5	300.1	-2	0	2
				2	0	2
				-2	0	-2
				2	0	-2
0.2873	3.481	301.3	276.2	-2	-2	1
				-2	2	1
				2	-2	1
				2	2	1
				-2	-2	-1
				-2	2	-1
				2	-2	-1
				2	2	-1
0.2992	3.342	255.3	248.8	-2	-1	2
				-2	1	2
				2	-1	2
				2	1	2
				-2	-1	-2
				-2	1	-2
				2	-1	-2
				2	1	-2
0.3281	3.048	190.8	217.5	-4	0	1
				4	0	1
				-4	0	-1
				4	0	-1
0.3285	3.044	189.3	216.3	-1	-3	0
				-1	3	0
				1	-3	0
				1	3	0
0.3345	2.989	183.7	208.9	-3	-2	1
				-3	2	1
				3	-2	1
				3	2	1
				-3	-2	-1
				-3	2	-1
				3	-2	-1
				3	2	-1
0.3066	3.262	242.5	239.7	-4	0	0
				4	0	0
0.3134	3.191	230.0	231.5	-3	-2	0
				-3	2	0
				3	-2	0
				3	2	0
0.3163	3.161	221.9	228.7	0	-2	2
				0	2	2
				0	-2	-2
				0	2	-2
0.3245	3.081	197.9	221.8	-4	--1	0
				-4	1	0
				4	-1	0
				4	1	0
0.3255	3.072	196.5	220.8	-1	-2	2
				-1	2	2
				1	-2	2
				1	2	2
				-1	-2	-2
				-1	2	-2
				1	-2	-2
				1	2	-2
0.3402	2.940	179.2	195.3	0	-3	1
				0	3	1
				0	-3	-1
				0	3	-1
0.3448	2.900	179.0	188.8	-3	-1	2
				-3	1	2
				3	-1	2
				3	1	2
				-3	-1	-2
				-3	1	-2
				3	-1	-2
				3	1	-2
0.3450	2.899	179.0	186.7	-4	-1	1
				-4	1	1
				4	-1	1
				4	1	1
				-4	-1	-1
				-4	1	-1
				4	-1	-1
				4	1	-1

The simulated two-dimensional WAXD patterns were compared with the observed patterns. Figure 6 shows the observed and simulated WAXD patterns at strain 6.0 for NR and IR at −50 °C. The WAXD patterns for other strains look similar and are not shown here. In all these images, the top and bottom portions of the images represent the observed and simulated WAXD pattern, respectively. It is to be noted that the observed images were the Fraser corrected images, where a portion of the (002) peak information may be lost. On the other hand, the simulation can produce the full (002) crystal

dx.doi.org/10.1021/ma400420k | *Macromolecules* 2013, 46, 4520−4528

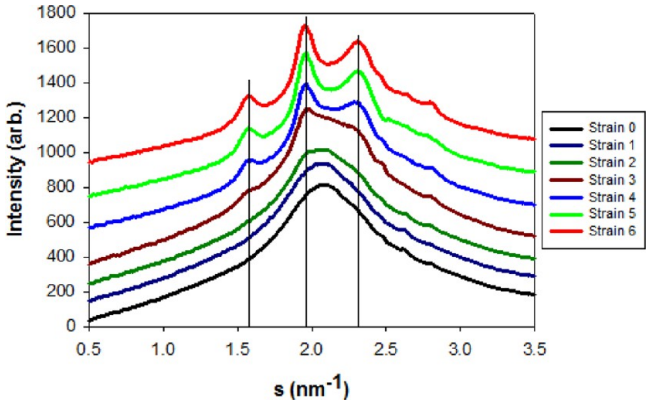

Figure 4. One-dimensional integrated intensities of NR at −50 °C at various strains. From strains 0.0 to 3.0, the amorphous halo is observed. From strains 4.0 to 6.0, both the crystal peaks and amorphous halo are observed.

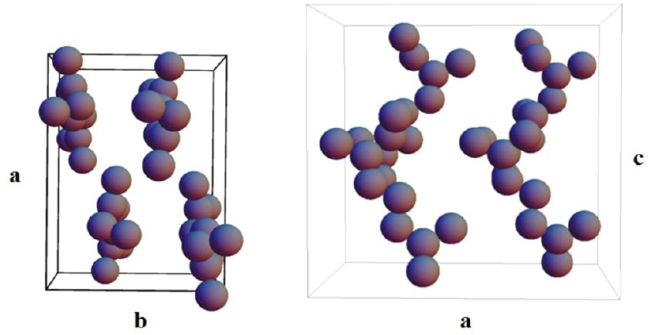

Figure 5. Orthorhombic unit cell of *cis*-1,4-polyisoprene with $P2_12_12_1$ symmetry. The unit cell dimensions are a = 13.048 Å, b = 9.391 Å, and c = 8.551 Å. These carbon atom coordinates are modified Rajkumar's coordinates.

peak and information on the crystallite size of the *c*-axis can be determined. From Figure 6, it is clear that the simulated WAXD image demonstrate an excellent fit to the experimental image for both samples. The different shapes of peaks in NR and IR are simulated, such as crescent and round, based on crystallites size and orientation.

Since the two-dimensional patterns show a good agreement between the simulated and observed, it is also important that it fits well in the one-dimensional space. Figure 7a shows the one-dimensional integrated intensity profile of the experimental (solid line) and simulated (long dashed line) WAXD pattern at strain 6.0 for NR and IR at −50 °C. The small dashed lines represent the separated simulated peaks of the total integrated intensity, which is composed of the amorphous halo (fitted using three Gaussian peaks) and oriented crystalline peaks.

In order to determine the goodness of fit between the simulation and observed, the standardized residuals and R^2 values were calculated. The standardized residual is defined as $(I_{sim} - I_{obs})/\sigma$, where I_{sim} and I_{obs} are the intensities obtained from the simulation and observed respectively, and σ is the standard deviation. Figure 7b shows the one-dimensional standardized residual plots calculated from the difference between the simulation and observed intensities in Figure 7a. The R^2 values were calculated for these fittings for NR and IR at −50 °C to be 0.988 and 0.986 respectively. The residual plots show random patterns with no trends, which indicate a good fitting of our simulation intensities to the observed.

Crystalline Fraction. The crystalline fractions were determined from the one-dimensional integrated profiles of the simulated WAXD patterns by taking the ratio of integrated areas of the crystal peaks to the total integrated area. The crystalline fraction increases with strain as shown in Figure 8. NR at −50 °C has the larger crystalline fraction than IR at any strain, and this tendency have been reported in vulcanized NR and IR at +25 °C.[31−33] Therefore, it is noteworthy that the difference in SIC between NR and IR is prevailed from −50 to +25 °C, in both the vulcanized and unvulcanized state. The onset strain (initial strain where crystallization start to be observed) of crystallization can be determined from the best fit curve applied to each sample by extrapolating the plot of crystalline fraction versus strain to the crystalline fraction at 0% position. The crystalline fraction starts at strain 1.61 in NR and strain 3.97 in IR.

Crystallite Size −. Conventional one-dimensional WAXD analysis to determine lateral crystallite sizes (L) includes the use of the Scherrer's equation, i.e., $L_{hkl} = K\lambda/(\beta \cos \theta)$. Because Scherrer's equation uses the averaged one-dimensional integrated WAXD intensity, this equation leads to some

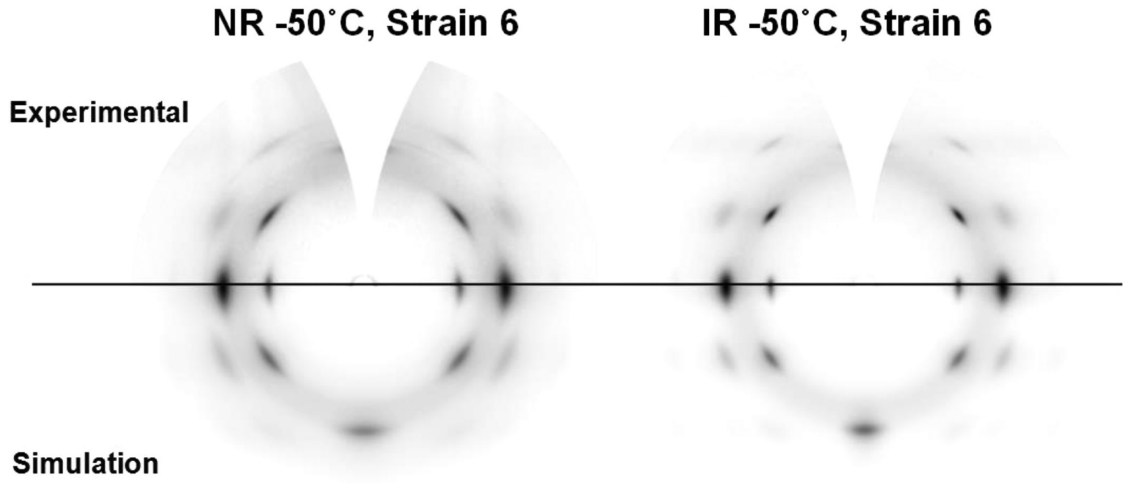

Figure 6. Two-dimensional observed and simulated WAXD patterns at strain 6.0 for NR and IR at −50 °C. The top and bottom portions of the images represent the observed and simulated WAXD pattern, respectively.

dx.doi.org/10.1021/ma400420k | *Macromolecules* 2013, 46, 4520−4528

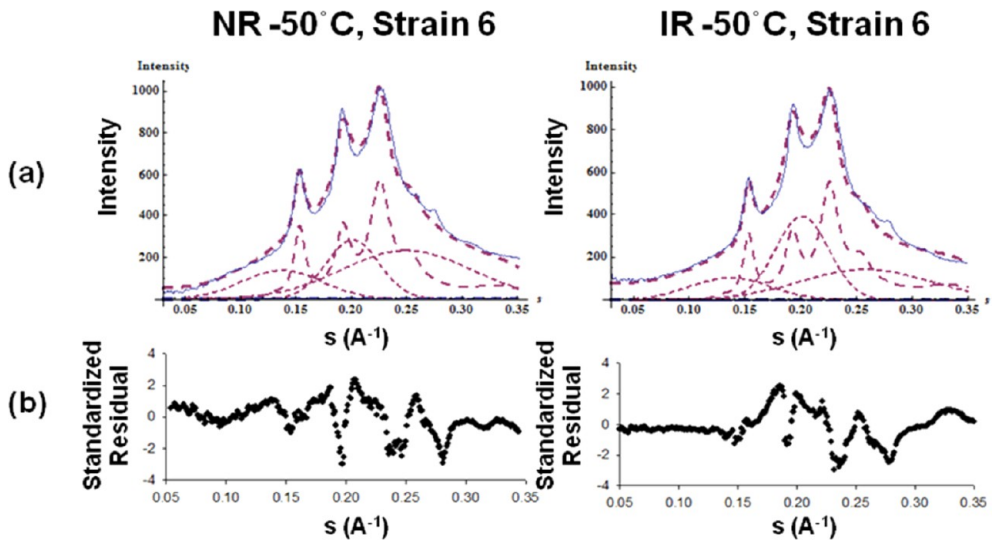

Figure 7. (a) One-dimensional integrated intensity profile of the observed (solid line) and simulated (long dashed line) WAXD pattern at strain 6.0 for NR and IR at −50 °C. The separated simulated peaks are shown in small dash lines. (b) One-dimensional standardized residual plots calculated from the difference between the simulation and observed intensities in part a.

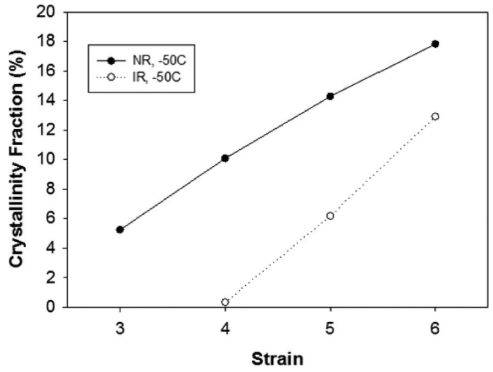

Figure 8. Crystalline fraction as a function of strain for NR and IR at −50 °C. The onset strains of SIC in NR and IR are 1.61 and 3.97, respectively.

limitations and inaccuracies in determining crystallite sizes. This averaged intensity approach typically contains closely spaced peaks that are partially blended together, such as (200) blended with (110), and (120) blended with (020) as shown in Table 1. Therefore, it can be difficult to separate these peaks and determine the exact peak widths, leading to inaccurate determinations of the apparent crystallite sizes. Furthermore, a peak-broadening effect can also be attributed to microstrains (or other types of lattice disorder) and instrumental effects. All these effects must be accounted for in order to obtain accurate crystallite sizes. Another major inaccuracy of the Scherrer equation is the determination of the true value of *K*. The value of *K* is determined by the shape of the crystal and influences how the width is determined. Typical *K* values for natural rubber have been reported to range from 0.8 to 1.0, where 1.0 signifies a perfectly symmetric peak shape profile. The values in this range essentially assume spherical crystals which may not be an accurate description for the present more anisotropic situation.

In the new two-dimensional simulation approach, exact scattering angles are defined and do not require the use of the true value of *K*. For the simulated WAXD patterns, the lateral crystallite sizes were estimated from taking the reciprocal value of the width, w, obtained in eq 8. The lateral crystallite sizes were estimated using the (*200*) and (*120*) diffraction peaks. Figure 9a shows the lateral crystal sizes for (*200*) and (*120*) diffraction peaks as a function of strain for NR and IR at −50 °C. For all the samples, the lateral crystallite size decreased only

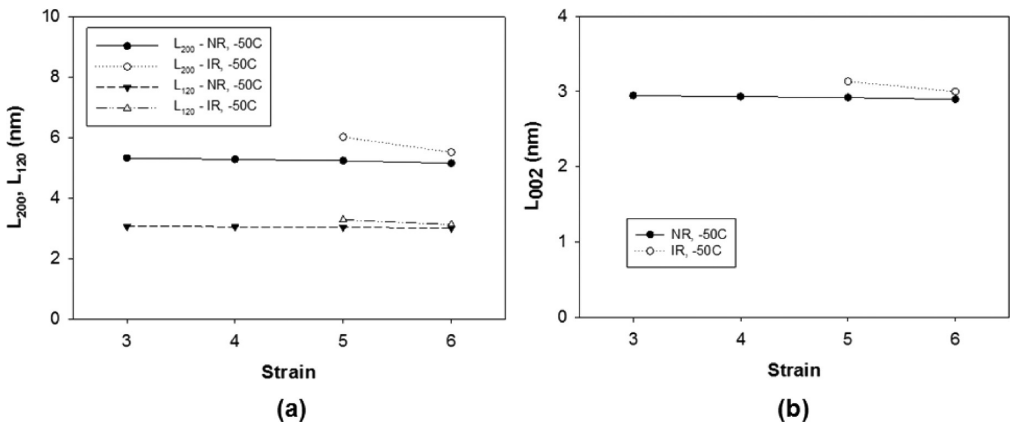

Figure 9. Crystallite sizes of the (*200*), (*120*), and (002) diffraction peaks as a function of strain for NR and IR at −50 °C.

dx.doi.org/10.1021/ma400420k | *Macromolecules* 2013, 46, 4520−4528

slightly with increasing strain, even up to strains 6. The unit cell contracts slightly in the direction perpendicular to the deformation (the *a*- and *b*-directions), as Trabelsi et al.[14] and Tosaka et al.[15] reported. The size of the (*200*) crystallite is almost doubled that of the (*120*) crystallite. The *c*-axis crystallite size can be estimated using the (002) diffraction peak and shown in Figure 9b. The size in the *c*-axis seems to be not changed in spite of being extended to this direction. The crystallites sizes do not seem to be changed. They are almost constant as Trabelsi reported, although they used Scherrer's equation. Since the crystallite sizes are almost constant, the larger crystalline fraction is attributed to the increase of the number of crystallites. From the width of L_{200}, L_{120}, and L_{002}, the crystallites dimensions are calculated as 5.51 nm × 3.12 nm × 3.00 nm in the *a*, *b*, and *c* direction respectively. This may suggests that there are around four unit cells in the crystallites along the three directions. The size is very small as compared to the dimensions at +25 °C.[14,15] We will report the dimensions at higher temperature elsewhere.

Crystallite Orientation. The crystallite orientations throughout deformation were determined using the Hermans' orientation parameter (P_2) in eq 6. The comparison of the P_2 orientation factors with respect to strain for NR and IR at −50 °C is shown in Figure 10. The orientation increases with strain

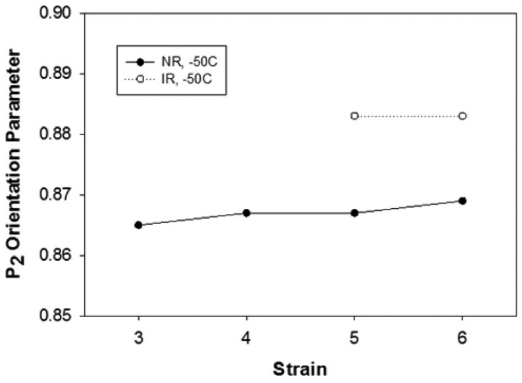

Figure 10. P_2 orientation of the crystallites as a function of strain for NR and IR at −50 °C.

and approaches a value close to 1, which indicates the increase in alignment of crystallites along the stretching direction during deformation. The orientation of IR is higher than NR at −50 °C. We (along with previous researchers) assumed that SIC are completely parallel to the extension direction and fiber symmetry. But this result suggest that SIC are not completely aligned and NR seems to have more constraint to be parallel than IR. These phenomena must be accelerated at −50 °C since molecules are more rigid than at +25 °C. The results can be expected from Figure 2, since NR peaks have shapes that are crescent and IR peaks are round. The difference between NR and IR may be caused by pseudo network and impurities in NR, such as the large crystals of quebrachitol and stearic acid, and big agglomerates including proteins and phospholipids.

Displacement Disorder in Crystal. A plot of the Debye−Waller factor, *B*, in eq 7 with respect to strain for NR and IR at −50 °C is shown in Figure 11. The value of *B* decreases with strain, which is an indication of higher order at large strains. This is consistent with the increase in orientation with strain as shown in Figure 10. Therefore, crystallites become oriented and less disordered during extension. The magnitude of disorder is

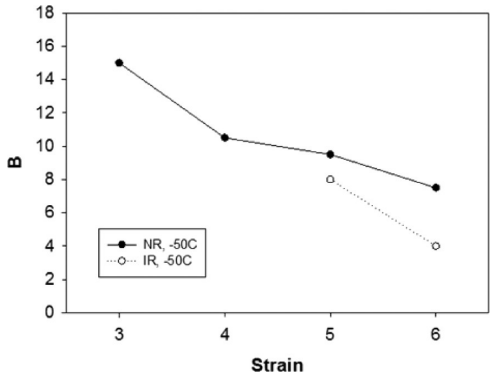

Figure 11. Debye−Waller factor, *B*, as a function of strain for NR and IR at −50 °C.

around a few angstroms according to the *B* value, since *B* can be expressed as $2\pi^2/3 \times \Delta u^2$, where Δu is the displacement of atoms in the case of an ideal free lattice and atoms can move independently from unit cell.[26] In the case of polymer crystals, there are defects/dislocations located inside of the crystals and folding of chains located on the surface. Therefore, the structure disorder may contribute to the *B* factor. We consider the value of *B* as a measure of disorder of SIC. The NR samples have a higher *B* as compared to IR at −50 °C. This is against the fact that NR is composed of a more perfect stereoregularity (100%) of *cis*-1,4-polyisoprene than IR (98.5%). The non-rubber components and pseudo network in NR may lead to more constraints that may affect the *B*-factor. SIC in NR may be activated by the pseudonetwork or nonrubber components rather than perfect stereoregularity.

Proposed SIC Model. From the two-dimensional WAXD simulations, we found the same unit cell dimensions for both NR and IR at −50 °C and have showed an excellent agreement between the simulation and observed results. The average number amount of unit cells per crystallite (*n*) in the *a*, *b*, and *c* direction (denoted as *a* × b × c) were determined from the unit cell lattice constants and the lateral crystallite sizes. Since the crystallite sizes and unit cell constants of NR and IR at −50 °C were almost identical even up to strain 6.0, they both contain 4 × 4 x 4 unit cells per crystallite at −50 °C. Only the crystallite size for NR at −50 °C is shown in Figure 12. The model for IR at −50 °C looks similar, but with smaller amounts of crystallites since the crystalline fraction is smaller than NR at −50 °C.

CONCLUSION

A new two-dimensional simulation approach has been presented to generate the WAXD patterns for SIC of unvulcanized NR and IR at −50 C. The calculated scattering intensities based on the modified atomic coordinates of Rajkumar et al. are very close to our observed data. We concluded that the unit cell of SIC is orthorhombic, $P2_12_12_1$ symmetry, with lattice constants of *a* = 13.04 Å, *b* = 9.39 Å, and *c* = 8.55 Å. The dimensions of unit cell of NR and IR are the same and do not change during deformation.

The simulation of 2D WAXD images with the width of crystallites *w*, the orientation of crystallites p, the crystal disorder B, following calculated scattering intensities depict the observed 2D scattering patterns successfully. The different styles of peaks in NR and IR (crescent and round) are caused by crystallites dimension and orientation. IR crystallites are

dx.doi.org/10.1021/ma400420k | *Macromolecules* 2013, 46, 4520−4528

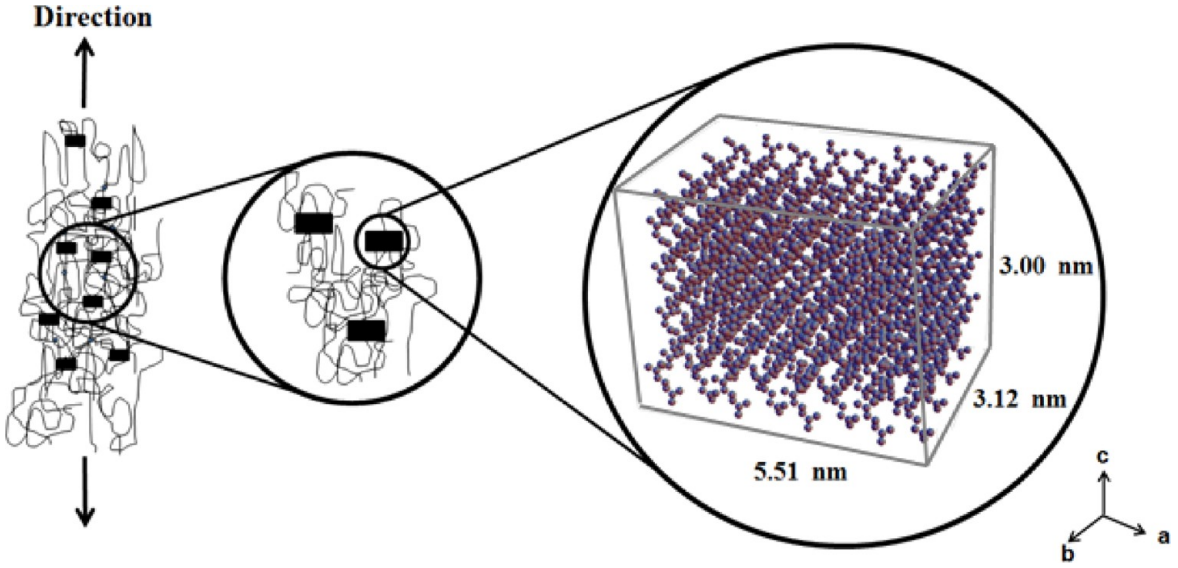

Figure 12. Model of the average crystallite size for the SIC of unvulcanized NR at −50 °C.

more aligned toward the extension direction than NR crystallites. The sizes of crystallites do not change during extension. The increase of crystalline fraction is attributed to the increase in the number of crystallites during extension. The order of crystal in NR is lower than in IR, which suggests that the different behavior of SIC in NR and IR is caused by pseudo network rather than stereoregularity.

AUTHOR INFORMATION

Corresponding Author

*E-mail: (J.C.) justinche1@gmail.com; (C.B.) ch.burger@gmail.com; (S.T.) shigeyukitoki@gmail.com.

Notes

The authors declare no competing financial interest.

ACKNOWLEDGMENTS

J.C., C.B., S.T., L.R., and B.S.H. acknowledge the financial support from the National Science Foundation (DMR-0906512). J.C. would like to acknowledge Diane Colabello for the TOPAS software analysis. S.A. and J.S. acknowledge the financial support by the Thailand Research Fund PHD/0142/2546, the Center of Excellence for Innovation in Chemistry (PERCH−CIC), the Commission on Higher Education RMU4980046. S.A. would like to acknowledge the Yokohama Rubber Co., Ltd., and Thai Rubber Latex Co. for their kind support in various ways.

REFERENCES

(1) Katz, J. R. *Kolloid Z.* **1925**, *36*, 300.
(2) Katz, J. R. *Kolloid Z.* **1925**, *37*, 10.
(3) Mark, H.; von Susich, G. *Kolloid Z.* **1928**, *46*, 11.
(4) Morss, H. A., Jr *J. Am. Chem. Soc.* **1938**, *60*, 237.
(5) Bunn, C. W. *Proc. R. Soc. London A* **1942**, *180*, 40.
(6) Nyburg, S. C. *Acta Crystallogr.* **1956**, *7*, 385.
(7) Natta, G.; Corradini, P. *Angew. Chem.* **1956**, *68*, 615.
(8) Takahasi, Y.; Kumano, T. *Macromolecules* **2004**, *37*, 4860.
(9) Immirzi, A.; Tedesco, C.; Monaco, G.; Tonelli, A. E. *Macromolecules* **2005**, *38*, 1223.
(10) Rajkumar, G.; Squire, J. M.; Arnott, S. *Macromolecules* **2006**, *39*, 7004.
(11) Gent, A. N. *Trans. Faraday Soc.* **1954**, *50*, 521.
(12) Mitchell, G. R. *Polymer* **1984**, *25*, 1563.
(13) Toki, S.; Sics, I.; Ran, S.; Liu, L.; Hsiao, B. S.; Murakami, S.; Senoo, K.; Kohjiya, S. *Macromolecules* **2002**, *35*, 6578.
(14) Trabelsi, S.; Albuoy, P. A.; Rault, J. *Macromolecules* **2003**, *36*, 7624.
(15) Tosaka, M.; Murakami, S.; Poompradub, S.; Kohjiya, S.; Ikeda, Y.; Toki, S.; Sics, I.; Hsiao, B. S. *Macromolecules* **2004**, *37*, 3299.
(16) Tosaka, M.; Senoo, K.; Sato, K.; Noda, M.; Ohta, N. *Polymer* **2012**, *53*, 864.
(17) Flory, P. J. *J. Phys. Chem.* **1947**, *15*, 397.
(18) Mitchell, J. C.; Meier, D. J. *J. Polym. Sci.* **1968**, *6*, 1689.
(19) Tosaka, M.; Kawakami, D.; Senoo, K.; Kohjiya, S. *Macromolecules* **2006**, *39*, 5100.
(20) Tanaka, Y. *Rubber Chem. Technol.* **2001**, *74*, 355.
(21) Karino, T.; Ikeda, Y.; Yasuda, Y.; Kohjiya, S.; Shibayama, M. *Biomacromolecules* **2007**, *8*, 693.
(22) Amnuaypornsri, S.; Toki, S.; Hsiao, B. S.; Sakdapipanich, J.; Tanaka, Y. *Rubber Chem. Technol.* **2008**, *81*, 753.
(23) Toki, S.; Burger, C.; Hsiao, B. S; Amnuaypornsri, S.; Sakdapipanich, J.; Tanaka, Y. *J. Polym. Sci., Part B: Polym. Phys.* **2008**, *46*, 2456.
(24) Burger, C.; Hsiao, B. S.; Chu, B. *Polym. Rev.* **2010**, *50*, 91.
(25) Burger, C.; Zhou, H.; Sics, I.; Hsiao, B. S.; Chu, B.; Graham, L.; Glimcher, M. J. *J. Appl. Crystallogr.* **2008**, *41*, 252.
(26) Mao, Y.; Burger, C.; Zuo, F.; Hsiao, B. S.; Mehta, A.; Mitchell, C.; Tsou, A. H. *Macromolecules* **2011**, *44*, 558.
(27) Ruland, W. *Colloid Polym. Sci.* **1977**, *255*, 833.
(28) Guinier, A. X-Ray Diffraction: In Crystals, *Imperfect Crystals, and Amorphous Bodies*; W. H. Freeman: San Francisco, CA, and London, 1963.
(29) Sears, V. F.; Shelley, S. A. *Acta Crystallogr.* **1991**, *47*, 441.
(30) Fraser, R. D. B.; Macrae, T. P.; Miller, A.; Rowlands, R. J. *J. Appl. Crystallogr.* **1976**, *9*, 81.
(31) Toki, S.; Fujimaki, T.; Okuyama, M. *Polymer* **2000**, *41*, 5423.
(32) Toki, S.; Sics, I.; Ran, S.; Liu, L.; Hsiao, B. S.; Murakami, S.; Senoo, K.; Kohjiya, S. *Polymer* **2003**, *44*, 6003.
(33) Toki, S.; Sics, I.; Hsiao, B. S.; Murakami, S.; Tosaka, M.; Poompradub, S.; Kohjiya, S.; Ikeda, Y. *J. Polym. Sci., Part B: Polym. Phys.* **2004**, *42*, 956.